Circular Unit Cell Gratings for X-ray Dark-Field Imaging

Kagias, Matias ; Pandeshwar, Amogha ; Wang, Zhentian ; Villanueva-Perez, Pablo ; Jefimovs, Konstantins ; Stampanoni, Marco

Abstract: Dark-field imaging has been demonstrated to provide complementary information about the unresolved microstructure of the investigated sample. The usual implementation of a grating interferometer, which can provide access to the dark-field signal, consists of linear gratings limiting the sensitivity to only one direction (perpendicular to the grating lines). Recently, a novel grating design, composed of circular unit cells, was proposed allowing 2D-omnidirectional dark-field sensitivity in a single shot. In this work we present a further optimisation of the proposed grating by changing the arrangement of the unit cells from a Cartesian to a hexagonal grid. We experimentally compare the two designs and demonstrate that the latter has an improved performance.

DOI: https://doi.org/10.1088/1742-6596/849/1/012053

Journal of Physics: Conference Series

Circular Unit Cell Gratings for X-ray Dark-Field Imaging

IOP Conf. Series: Journal of Physics: Conf. Series **849** (2017) 012053 doi:10.1088/1742-6596/849/1/012053

Circular Unit Cell Gratings for X-ray Dark-Field Imaging

Matias Kagias[1,2], Amogha Pandeshwar[2], Zhentian Wang[1,2], Pablo Villanueva-Perez[1,2], Konstantins Jefimovs[1], and Marco Stampanoni[1,2]

1)Swiss Light Source, Paul Scherrer Institute, Villigen, Switzerland
2)Institute for Biomedical Engineering, University and ETH Zurich, Zurich, Switzerland

Abstract. Dark-field imaging has been demonstrated to provide complementary information about the unresolved microstructure of the investigated sample. The usual implementation of a grating interferometer, which can provide access to the dark-field signal, consists of linear gratings limiting the sensitivity to only one direction (perpendicular to the grating lines). Recently, a novel grating design, composed of circular unit cells, was proposed allowing 2D-omnidirectional dark-field sensitivity in a single shot. In this work we present a further optimisation of the proposed grating by changing the arrangement of the unit cells from a Cartesian to a hexagonal grid. We experimentally compare the two designs and demonstrate that the latter has an improved performance.

1. Introduction

Grating interferometry (GI) is a phase and scattering sensitive method capable of providing complementary information to standard absorption imaging of a sample [1, 2, 3]. A number of different possible applications have been unlocked by these capabilities, covering both the industrial [4] and medical fields [5, 6]. The main strength of scattering or so called dark-field imaging is that it can reveal information about the unresolved microstructure of the investigated sample [7, 8, 9, 10, 11]. The usual realisation of a grating interferometer is based on linear gratings. Such a design allows differential phase and dark-field sensitivity in only the direction perpendicular to the grating lines. In the case of samples with highly anisotropic scattering properties, a strong correlation of the retrieved dark-field signal and the relative orientation of the grating lines and the sample can be observed [12]. In order to achieve a more complete understanding of the unresolved microstructure multiple measurements by rotating the sample or the interferometer are necessary [13]. Recently, a method based on a single phase grating, capable of being sensitive to scattering in all the directions of the imaging plane has been proposed [14]. This was achieved by utilising a phase grating that is composed by a mosaic repetition of circular gratings. We will call this kind of design as square packing of circular unit cells. The circular design of the unit cells allows 2D-omnidirectional sensitivity, by repeating the unit cells the omnidirectional sensitivity can be obtained over the full field of view (FOV). The omnidirectional images that are obtained have a pixel matrix defined by the mosaic repetition of the unit cells. A square packing of the unit cells is undoubtedly the most straightforward implementation of such a grating design since the layout of the unit cells defines the pixel matrix. However, such an implementation comes with a number of limitations. A square packing of circles on a plane does not have an optimum fill factor since dead space is created in the corners

of the cells. Moreover, each unit cell will interfere with its neighbouring, therefore it is favourable that the layout has as many axes of symmetry as possible in order to increase the uniformity of the resulting interference pattern. A hexagonal packing of the unit cells has a higher fill factor and more axes of symmetry than square packing. In this work, we fabricate such a grating and perform experimental comparison to demonstrate the improved performance of the design.

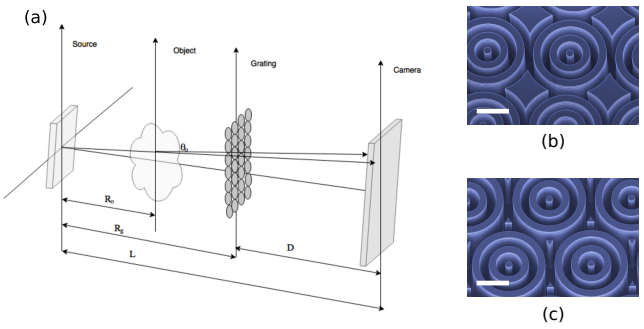

Figure 1. (a) Schematic of the used setup. (b) SEM image of the square packed grating (SPG). (c) SEM image of the hexagonally packed grating. The scale bar both in (b) and (c) is 10 μm

2. Materials and methods

The method in use has been fully documented and developed in [14]. The key points of [14] are repeated here for clarity. A general schematic representation of the setup is shown in figure 1 (a). The proposed grating design exploits its local circular symmetry in order to achieve a sensitivity in all the directions of the imaging plane. In more detail, the interference fringe is recorded with sufficient resolution and then analysed. The phase grating is designed to introduce a phase shift of $\pi/2$ for the X-ray wavelength λ. For a grating period g_1 the intensity interference pattern can be observed at the following distances from the grating

$$D_n = n\frac{g_1^2}{2\lambda}, n = 1, 3, ... \tag{1}$$

In order to observe the interference pattern at these distances sufficient coherence is required. There is a direct connection between beam coherence and fringe visibility of the interference pattern. When a scattering sample is introduced the angular distribution of the beam will be broadened which in turn will cause a reduction in the visibility of the pattern. By checking the visibility reduction at every angle of each circular pattern directional dark-field images can be produced.

The experimental procedure consists of recording two images, one with only the grating in the beam (flat), and one with the grating and the sample (sample). The analysis of the recorded images can be broken down into the following steps. Initially, the generated interference fringe is recorded. A unit cell finding algorithm is then used to detect and crop out each cell. The detection criterion is based on the maximum intensity that is observed in the centre of the cell due to the circular symmetry [15]. The next step consists of transforming each unit cell from cartesian to polar coordinates, symmetry criteria can be used to yield a more accurate interpolation than a direct conversion of coordinates. Finally, the visibility reduction is calculated for each angle.

The square packing (SPG) of the circular unit cells has a fill factor of $\frac{\pi}{4} \approx 0.785$. If the unit cells are arranged in a honeycomb manner (hexagonal packing) (HPG) the packing ratio increases to $\frac{\pi}{2\sqrt{3}} \approx 0.906$ leading to a higher unit cell density in the final image. This will result in a higher photon utilisation for dark field imaging.

To evaluate the performance of the proposed hexagonal packing in comparison to the previously used square packing we fabricated gratings with the two different designs. The two designs have an identical period g_1 and each unit cell contains the same number of periods. Both gratings are fabricated on the same Si chip, allowing easy processing but also a straightforward change of grating during the experiment. Scanning electron microscopy images (SEM) of the fabricated gratings can be seen in figures 1 (b) and (c).

3. Results

Two types of experiments were performed to compare the two grating designs. The first one was a straightforward comparison of the angular visibility of the flat images. The second comparison focused on the angular sensitivity that each grating can achieve for a known scattering sample. The sample was composed of 0.6 μm wide Au lines in Si that were repeated with a period of 1.3 μm. The Au lines are expected to scatter in the direction perpendicular to them. The sample was rotated covering the angles for 0^o to 180^o with a step size of 1^o. By using a model proposed in [12] the direction of the lines and consecutively the scattering direction was estimated. We call this the most prominent scattering direction (MPSD). The standard deviation of the distribution of angles over the FOV was used as an accuracy merit of the estimation.

The experiments were performed at the TOMCAT beamline [16], of the Swiss Light Source, Switzerland. The selected energy was 25 keV to minimise the absorption of the Au lines. The gratings were fabricated in-house with the following parameters: period 5μm, 25μm unit to unit distance and 17μm depth. A 20 μm thick LuAG:Ce scintillator coupled with a 10 fold objective was placed 25 cm from the phase grating. The magnified visible light image was then recorded by a pco.edge 4.2 CMOS camera. The effective pixel size was 0.65 μm which allowed the recording of the 5 μm period fringes.

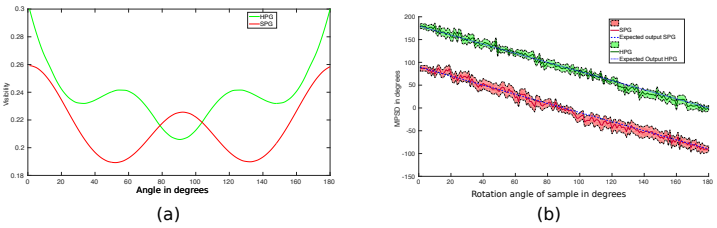

Figure 2. (a) Visibility curves for HPG and SPG. (b) MPSD distributions for SPG and HPG.

The calculated visibilities for each grating design are shown in figure 2 (a). Both visibilities depend on the angle, and two reasons contribute to this modulation. First, the photon source is not symmetric and therefore it is expected to have different visibilities in x and y directions. Secondly and most importantly the configuration of the unit cells play a vital role in the angular visibility. In the case of SPG (red line) we expect maxima at 0^o, and 90^o and minima at 45^o and 135^o which are observed in our experimental measurements. Analogously, for the HPG we expect maxima at 0^o, 60^o, and 120^o and minima at 30^o, 90^o, and 150^o. In figure 2 (b) we compare the estimated most prominent scattering direction (MPSD) again for both designs. It should be noted that the curves are shifted by 90^o in order to make the comparison easier. The width of the bands follows the visibility curves, on average the HPG delivered 25% higher angular sensitivity compared to the SPG. To close, we show an imaging example of a trabecular bone sample embedded in PMMA. In figure 3 (b) and (c) we can see the estimated scattering angle for the SPG and HPG respectively. The noise is reduced in the case of the HPG. For completeness the transmission image is shown in figure 3 (a).

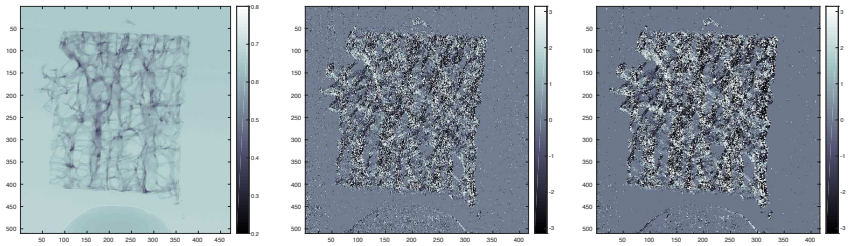

Figure 3. (a) Transmission and maximum scattering angles for SPG (b) and HPG (c) of trabecular bone sample.

4. Conclusion

Two gratings designs for 2D-omnidirectional dark-field imaging were compared. The hexagonally packed grating (HPG) had an improved visibility compared to the square packed one. Additionally, the angular sensitivity was improved by 25% by switching to the HPG. This change in the design of the grating can boost the performance of the method and increase its applicability in more demanding applications.

5. Acknowledgments

Part of this work has been supported by ERC Grant No. ERC-2012-StG 310005-PhaseX. We would like to thank Dr. Marios Georgiades for providing the bone sample.

References

[1] T. Weitkamp, A. Diaz, C. David, F. Pfeiffer, M. Stampanoni, P. Cloetens and E. Ziegler, Opt. Express **13**, 6296-6304 (2005).
[2] A. Momose, S. Kawamoto, I. Koyama, Y. Hamaishi, K. Takai, and Y. Suzuki, Jpn. J. Appl. Phys. **42**, L866-L868 (2003).
[3] C. David, B. Nöhammer, H. H. Solak, and E. Ziegler, Appl. Phys. Lett. **81**, 3287-3289 (2002).
[4] V. Revol, I. Jerjen, C. Kottler, P. Schütz, R. Kaufmann, T. Lüthi, U. Sennhauser, U. Straumann, and C. Urban, J. Appl. Phys. **110**, 044912 (2011).
[5] M. Stampanoni, Z. Wang, T. Thüring, C. David, E. Roessl, M. Trippel, R.A. Kubic-Huch, G. Singer, M.K. Kohl, and N.Hauser, Invest. Radiol. **46**, 801-806 (2011).
[6] D. Stutman, T.J. Beck, J.A. Carrino, and C.O. Bingham, Phys. Med. Biol. **56**, 5697-5720 (2011).
[7] Z. Wang, and M. Stampanoni, Phys. Med. Biol. **60**, 4123-4135 (2015)
[8] Z. Wang, N. Hauser, G. Singer, M. Trippel, R.A. Kubik-Huch, C.W. Schneider, and M. Stampanoni, Nat. Commun. **5**, 3797 (2013).
[9] M. Bech, A. Tapfer, A. Velroyen, A. Yaroshenko, B. Pauwels, J. Hostens, P. Bruyndonckx, A. Sasov and, F. Pfeiffer, Sci. Rep. **3**, 3209 (2013).
[10] S. Schleede, F.G. Meinel, M. Bech, J. Herzen, K. Achterhold, G. Potdevin, A. Malecki, S. Adam-Neumair, S.F. Thieme, F. Bamberg, K. Nikolaou, A. Bohla, A. Ö. Yildirim, R. Loewen, M. Gifford, R. Ruth, O. Eickelberg, M. Reiser, and F. Pfeiffer, PNAS **109**(44), 17880-17885 (2012).
[11] K. Hellbach, A. Yaroshenko, F.G. Meinel, A.Ö. Yildirim, T.M. Conlon, M. Bech, M. Mueller, A. Velroyen, M. Notohamiprodjo, F. Bamberg, S. Auweter, M. Reiser, O. Eickelberg, and F. Pfeiffer, Invest. Radiol. **50**(7), 430-435 (2015).
[12] T.H. Jensen, M. Bech, O. Bunk, T. Donath, C. David, R. Feidenhans'l, and F. Pfeiffer, Phys. Rev. B **55**, 3317 (2010).
[13] T.H. Jensen, M. Bech, I. Zanette, T. Weitkamp, C. David, H. Deyhle, S. Rutishauser, E. Reznikova, J. Mohr, R. Feidenhans'l, and F. Pfeiffer, Phys. Rev. B **82**, 214103 (2010).
[14] M. Kagias, Z. Wang, P. Villanueva-Perez, and M. Stampanoni, Phys. Rev. Lett. **116**, 093902 (2016)
[15] D.E Silva, Appl. Opt. **11**, 2613-2624, (1972).
[16] M. Stampanoni, A. Groso, A. Isenegger, G. Mikuljan, Q. Chen, A. Bertrand, S. Henein, R. Betemps, U. Frommherz, P. Bohler, D. Meister, M. Lange, and R. Abela, AIP Conf. Proc., 879, 848 (2007).